Metamorphic narrow-gap InSb/InAsSb superlattices with ultra-thin layers

Maksim Ermolaev, Sergey Suchalkin, Gregory Belenky, Gela Kipshidze, Boris Laikhtman, Seongphill Moon, Mykhaylo Ozerov, Dmitry Smirnov, Stefan P. Svensson, and Wendy L. Sarney

---

Metamorphic narrow-gap InSb/InAsSb superlattices with ultra-thin layers

Maksim Ermolaev,[1] Sergey Suchalkin,[1,a)] Gregory Belenky,[1] Gela Kipshidze,[1] Boris Laikhtman,[2] Seongphill Moon,[3,4] Mykhaylo Ozerov,[3] Dmitry Smirnov,[3] Stefan P. Svensson,[5] and Wendy L. Sarney[5]

[1]State University of New York at Stony Brook, Stony Brook, New York 11794-2350, USA
[2]Racah Institute of Physics, Hebrew University, Jerusalem 91904, Israel
[3]National High Magnetic Field Laboratory, Tallahassee, Florida 32310, USA
[4]Department of Physics, Florida State University, Tallahassee, Florida 32306, USA
[5]U.S.Army Research Laboratory, 2800 Powder Mill Rd, Adelphi, Maryland 20783, USA

Metamorphic strain compensated $InSb/InAsSb_{0.52}$ superlattices (SLs) with ultrathin layers and different periods grown on GaSb substrate were designed, fabricated, and characterized. It was shown that a period increase from 3 to 6.2 nm reduced the effective bandgap energy from 70 to 0 meV. A further increase in the period leads to inversion of the valence and conduction bands. Magneto-optical experiments demonstrated that Dirac-like carrier dispersion is characteristic of almost gapless $InSb/InAsSb_{0.52}$ SLs. Indication of hole transport enhancement over that found in InAsSb/InAsSb SL structures is presented. *Published by AIP Publishing.* https://doi.org/10.1063/1.5051767

Fabrication of semiconductor devices operating at a wavelength of 8 μm and above requires narrow gap materials. In the case of III–V strained-layer superlattices (SLs) grown pseudomorphically on GaSb, the layer containing electrons must be very thick[1] in order to minimize the SL bandgap. This requirement leads to suppression of the hole transport and reduction of the optical absorption coefficient.[2]

The metamorphic approach for growth of virtual substrates on GaSb allows the lattice constant to be a design parameter and enables growth of bulk InAsSb as well as type II SLs with enhanced design flexibility which make them the best amongst the competing choices to HgCdTe for long and very-long wave optoelectronic applications.[3] The materials' effective bandgap can be tuned to values lower than the minimum bulk value of InAsSb by the use of high quality narrow band, strain compensated SLs with ultra-thin layers (short-period SLs)[4] that can be thought of as an ordered alloy. A SLS period can generally consist of $InAs_{1-x}Sb_x/InAs_{1-y}Sb_y$. The commonly used "Ga-free" SLS refers to the case $x > y = 0$. We have recently demonstrated the properties of the case $x > y > 0$. In this work, we use $x = 1$, $y > 0$ and present a short-period strain-compensated $InSb/InAsSb_{0.52}$ SL grown on a virtual substrate with an in-plane lattice constant of 6.33 A. Variation of the period thickness allows fabrication of a series of SL structures with bandgaps ranging from 70 meV down to zero and further to band inversion. Besides applications for far infra-red optoelectronics, the materials can serve as a new platform for observation of intriguing physical phenomena like Dirac carrier dispersion and non-trivial topological phases[5,6]

Increasing the As composition in the electron-containing layer and the Sb composition in the hole-containing layer leads to an increase in the type-II band discontinuity [Fig. 1(a)]. The discontinuity is further enhanced by the tensile strain in the electron-containing layers and the compressive strain in the hole-containing layers. The distribution of strain between the "electron" and "hole" layers is controlled by the lattice constant of the virtual substrate.

The pair of materials we have chosen for the SL layers allows us to reach almost the maximum type II discontinuity while maintaining manageable layer strain (Fig. 1). The SLs were grown by solid-source molecular beam epitaxy on undoped (100) GaSb substrates. The P-doped metamorphic buffer was graded from GaSb to $Al_{0.32}In_{0.68}Sb$ with a thickness of $\approx$2240 nm and an effective lattice constant of 6.33 A. $InAs_{0.48}Sb_{0.52}/InSb$ ordered alloys having a thickness of 1 μm and periods of 3, 4.7, 6.2, and 7.8 nm were sandwiched between 500 nm (bottom) and 200 nm (top) thick p-doped $Al_{0.67}In_{0.33}Sb$ barriers. The top barrier was covered with $\approx$30 nm of the corresponding ordered alloy as a cap layer. The $InAsSb_{0.52}$ layers are under 1% tensile strain and InSb layers are under $\sim$2% compressive strain. Strain balance was achieved with a layer thickness ratio of 2. The cap, both barriers, and the graded buffer are p-doped to 10^{16} cm^{-3} for all samples to avoid formation of 2D carrier "pockets" at the interfaces between the alloy layer and the barriers.[7] The crystalline quality of the samples was studied by high resolution x-ray diffraction (HRXRD) with a coupled 2Theta/Omega scan and transmission electron microscopy (TEM). Carrier concentrations were obtained from Hall measurements. The Hall bars were formed by wet etching down to the bottom barrier. Ohmic contacts were fabricated by deposition of Ni/Au/Ge/Ni/Au layers followed by rapid thermal annealing at 260 °C for 2 min and deposition of Ti/Pt/Au cover layers.

The energy band structure and bandgap were probed by magneto-optics measurements. Magnetic field dependence of the transmission spectra was obtained in the Faraday geometry. Samples were mounted in a cryostat equipped with a superconductive magnet. A Fourier-transform infrared (FTIR) spectrometer with a globar as an emission source and a Si bolometer was used to capture spectra. The substrate side of the samples was wedged to eliminate interference effects. Hall and magneto-optics measurements were performed at liquid He temperatures.

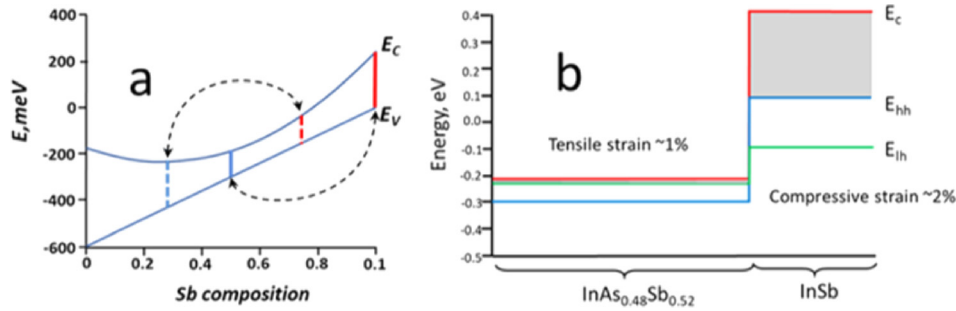a)Author to whom correspondence should be addressed: sergey.suchalkin@stonybrook.edu

FIG. 1. Conduction and valence band energies of $InAs_{1-x}Sb_x$ as a function of Sb composition x. The bowing of the valence band is neglected. The solid vertical red and blue lines correspond to the constituent layer materials of the $InSb/InAsSb_{0.52}$ SLs, and the dashed red and blue lines correspond to $InAsSb_{0.3}/InAsSb_{0.75}$[6] (a); Schematic band edge structure of a single period of SL with bulk electron (E_c), heavy hole (E_{hh}), and light hole (E_{lh}) energies of the SL materials. The gray area corresponds to the bandgap of bulk materials (b).
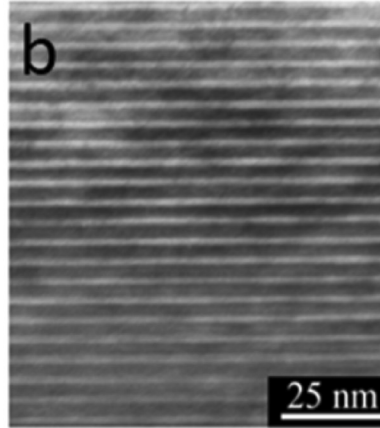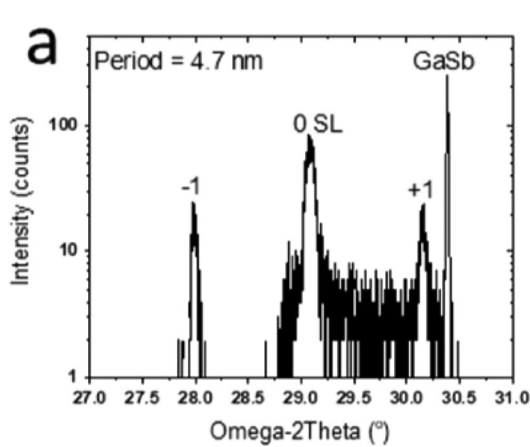

FIG. 2. Omega/2theta scan (a); TEM image of the sample with a period of 4.7 nm. Brighter lines correspond to InSb layers (b).

A 2Theta/Omega x-ray rocking curve for the SL with a period of 4.7 nm is shown in Fig. 2(a). Zero and first order peaks are well resolved, and their position is in agreement with the designed period of the samples. A TEM image [Fig. 2(b)] demonstrates a dislocation-free periodic structure with light layers corresponding to InSb layers and the dark ones corresponding to InAsSb.

Carrier concentrations obtained from Hall measurements for all samples were in the range of 1.11×10^{16} to 2.26×10^{16} cm^{-3} (Table I). Since it is very difficult to observe photoluminescence from ultralow bandgap materials, we used magneto-absorption to evaluate the SL bandgaps.

Relative transmission T(B)/T(0) spectra for samples with a period equal to 6.2 nm are presented as heat-maps with intensity indicated by color in Fig. 3.

A simple two-band kp model[8] was used to fit the experimental interband Landau level absorption lines. In this model, the in-plane spectrum of a narrow gap short period SL can be characterized with two parameters: SL bandgap E_g and Fermi velocity v_F

TABLE I. Carrier concentrations and experimental bandgaps for InSb/InAsSb$_{0.52}$ with different periods.

Sample #	Period, nm	Concentration, cm^{-3}	Eg, meV
1	3	2.26×10^{16}	~70
2	4.5	1.11×10^{16}	~40
3	6.2	1.43×10^{16}	~0
4	7.8	1.55×10^{16}	Inverted

$$E = \frac{E_g}{2} \pm \sqrt{\frac{E_g^2}{4} + v_F^2 \hbar^2 k_\parallel^2}. \qquad (1)$$

Here, E_g is the SL bandgap, formed by the ground electron and heavy hole subbands, v_F is the Fermi velocity, and zero energy is taken at the top of heavy hole subband. The Fermi velocity depends on the electron-hole envelop overlap and the average over the SL period momentum matrix element between electron and heavy hole subbands. The dashed lines in Figs. 3(a) and 3(b) are calculated intraband (CR) and interband optical transitions. There is another group of concurrent interband transition lines with an intercept energy of ~400 meV. The latter depends on the SL period so we attribute this feature to the optical transition between the first heavy hole sub-band and the ground electron sub-band.[9] This transition is parity-forbidden for $k_\parallel = 0$ but allowed for $k_\parallel = \frac{\pi}{d}$ in a type II Sl.[10] The calculated transition energy is close to the observed one. The detailed study of these features will be reported elsewhere.

Qualitatively, the magneto-absorption spectra are similar to those observed in narrow bandgap $InAsSb_{0.3}/InAsSb_{0.75}$ SLs.[6] This is expectable since in a nearly gapless SL, the in-plane spectrum is determined by just one parameter—v_F. The best fit is obtained with a Fermi velocity of $\approx 7.4 \times 10^5$ m/s which is ~10% higher than in the previously reported $InAsSb_{0.3}/InAsSb_{0.75}$. Since the interband momentum matrix elements are very close in InAs and InSb,[11] the difference can be accounted for by slightly different overlap between electron and hole states in the SL.
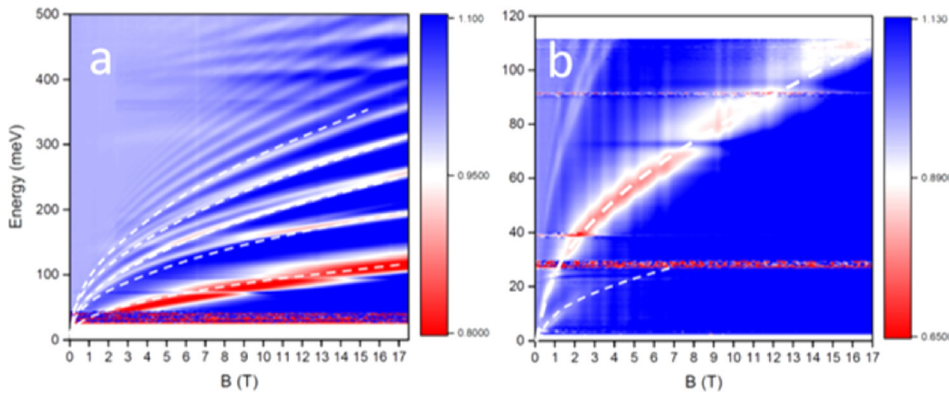
FIG. 3. Color plot of the relative transmission as a function of energy and magnetic field B for the SL with a 6.2 nm period in the Mid-IR (a) and Far-IR (b) spectral ranges. Red color corresponds to lower magnitude. The dashed lines are the calculated transition energies.
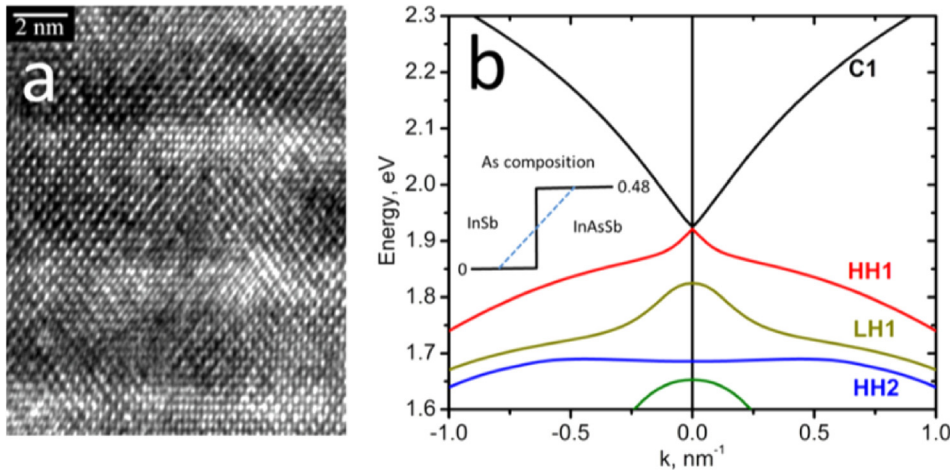

FIG. 4. High resolution TEM image of structure 2. Brighter areas correspond to InSb (a). Calculated band structure of an InSb/InAsSb$_{0.52}$ SL with a 6.2-nm period. Graded interfaces with an effective thickness of 2 nm were used for the model as shown in the inset (b).

The bandgaps, estimated from the energy axis intercept of the magnetic field dependence of the interband Landau level transition energies, are presented in Table I. The 8 band kp calculations[12] give bandgap values which are lower than the experimental ones.

For example, the zero bandgap crossing is calculated to take place for a SL period of 4.8 nm while the experiment indicates that the zero gap is reached at ~6.2 nm. A possible reason for this discrepancy is interface roughness[13] which is clearly seen in the high resolution TEM pictures [Fig. 4(a)] and a well-known problem in the InAs/InSb system.[14] In the first approximation, the interface roughness can be taken into account by the introduction of interfaces with a linearly graded composition [see the inset in Fig. 4(b)]. This will "soften" the SL ordering and make the material somewhat more resembling of the random ternary alloy with a bandgap of about ~100 meV. The effect of "smoothed out" interfaces will be more pronounced in a short period SL. To obtain nearly zero bandgap at the SL period of 6.2 nm, the effective interface width has to be around 2 nm.

The calculated in-plane dispersion for such a SL is shown in Fig. 4(b). The Fermi velocity calculated using data in Fig. 4 is $\approx 8.6 \times 10^5$ m/s, which is close to the experimental value. The CR and interband absorption lines in the SL with a period of 7.8 nm (Fig. 5) demonstrate nonzero intercept with the magnetic field axis, which is indicative of the bandgap inversion.[15]

One of the striking features of the structures is that in spite of the considerable interface roughness, the transitions between electron and hole Landau levels are resolved much

better than in a InAsSb$_{0.3}$/*InAsSb*$_{0.75}$ SL with the same period, while the cyclotron absorption lines have similar intensity and half-width. It is clearly seen in magneto-transmission spectra of structures with 4.5 nm and 6.2 nm periods shown in Fig. 6. The same effect was observed in all the structures.

The interface disorder provides a major mechanism of the elastic scattering in structures with narrow quantum wells.[16] It may have a different effect on the intraband magneto-absorption (cyclotron resonance) and interband transitions between electron and hole Landau levels. Qualitatively, the
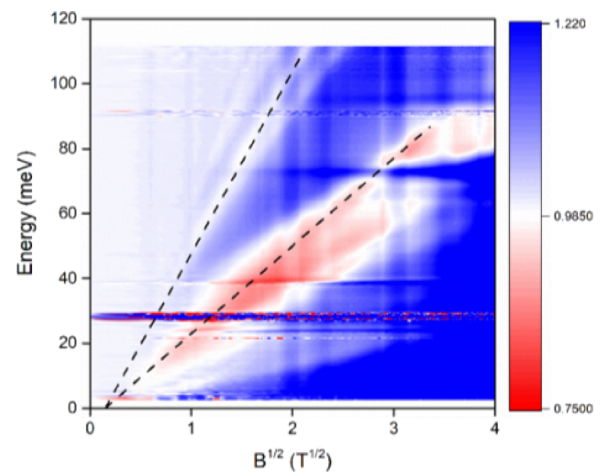

FIG. 5. Color plot of the relative transmission as a function of energy and square root of the magnetic field B for the InSb/InAsSb$_{0.52}$ SL with a 7.8-nm period in the Mid-IR.
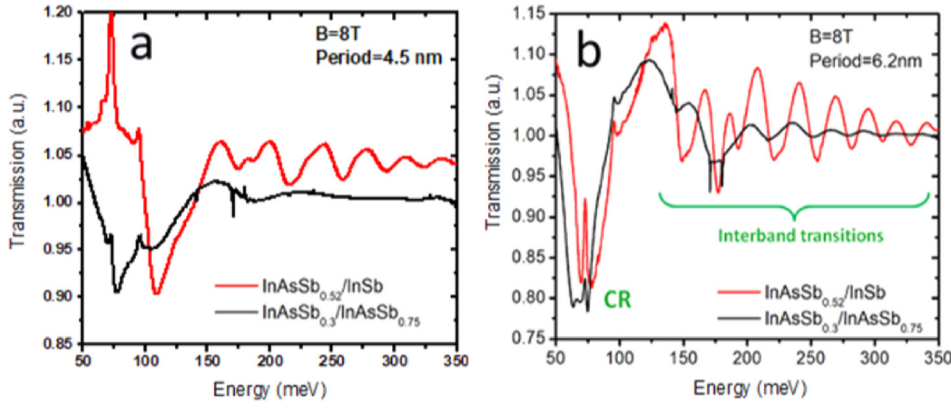
FIG. 6. Magneto-transmission spectra of the InSb/InAsSb$_{0.52}$ (red) and InAsSb$_{0.3}$/InAsSb$_{0.75}$ (black) SLs with 4.5 nm (a) and 6.2 nm (b).

interface roughness can be considered as a local random change in the SL layer width.

For a qualitative illustration, we used the approximation of smooth potential, i.e., the electron wavelength is less than the correlation length of the interface roughness profile. In the case of a SL with ultralow effective E_g, the Landau level energies can be expressed as

$$E_{e,n} \approx \frac{E_g}{2} + \frac{\hbar v_F}{l_B}\sqrt{2(n+1)} \qquad (2a)$$

for electrons and

$$E_{hh,n} \approx \frac{E_g}{2} - \frac{\hbar v_F}{l_B}\sqrt{2n} \qquad (2b)$$

for heavy holes. For simplicity, just one spin direction is considered. Here, n is the Landau level number, $l_B = \sqrt{\frac{\hbar c}{eB}}$ is the magnetic length, v_F can be expressed as $v_F = \frac{|P_{hh,e}|}{\sqrt{2}m_0}$,[6] and m_0 is the free electron mass. Interface roughness makes the E_g and v_F functions of the lateral coordinate r: $E_g, v_F \equiv E_g, v_F(r)$. However, lateral fluctuations of E_g do not contribute to the cyclotron resonance transition energy $E_{CR} = E_{e,2} - E_{e,1}$. This energy fluctuates only due to fluctuations of v_F. The latter depends on the local SL layer width even if the momentum matrix element in the adjacent SL layers is close. In this case, $|P_{hh,e}| \approx P \cdot I$[6] and

$$v_F \approx \frac{P}{\sqrt{2}m_0}I \approx 1.2 \cdot 10^6 \cdot I \left[\frac{m}{s}\right], \qquad (3)$$

where P in the momentum matrix element for InAs and GaSb, $\frac{2P^2}{m_0} \approx 22$ eV and $I \equiv \left|\int_0^d \xi_e(z)\xi_{hh}^*(z)dz\right|$ is the overlap between electron $\xi_e(z)$ and heavy hole states $\xi_{hh}(z)$ in the SL; z is the coordinate along the growth direction. The lateral fluctuations of the SL layer widths lead to fluctuations of the overlap between electrons and heavy holes and hence to fluctuations of v_F. Therefore, the fluctuations of the transition energies are

$$\delta E_{e,n1} - \delta E_{e,n2} = \frac{\hbar}{m_0 l_B}\left[\sqrt{n_1+1} - \sqrt{n_2+1}\right]P\delta I \qquad (4a)$$

for cyclotron resonance transition and

$$\delta E_{e,n1} - \delta E_{hh,n2} = \frac{\hbar}{m_0 l_B}\left[\sqrt{n_1+1} + \sqrt{n_2}\right]P\delta I \qquad (4b)$$

for interband transitions. It is obvious that the effect of the same interface roughness on the line width of interband transitions will be much stronger than on the line width of the cyclotron resonance due to the different sign in the square brackets. This difference of the line widths for cyclotron resonance and interband transitions will take place even beyond the approximation of long range roughness used to obtain Eqs. (4a) and (4b). since it comes from a strong correlation of the level fluctuations. This correlation is due to a strong intermixing between electron and hole states in a narrow gap SL. Landau level fluctuations in the same band are in phase, while for different bands, they are out of phase. This is explicitly seen in Eqs. (2a) and (2b).

In conclusion, metamorphic strain compensated InSb/InAsSb$_{0.52}$ SLs with ultrathin layers and different periods grown on the GaSb substrate were designed, fabricated, and characterized. It was shown that a period increase from 3 to 6.2 nm reduced the bandgap energy from 70 to 0 meV. A further increase in the period leads to inversion of the valence and conduction bands. Magneto-optical experiments demonstrated that almost gapless InSb/InAsSb$_{0.52}$ SLs are characterized by Dirac-like carrier dispersion. Evidence for the hole transport enhancement compared to InAsSb$_{0.3}$/InAsSb$_{0.75}$ structures was presented.

[1]A. Haddadi, G. Chen, R. Chevalier, A. M. Hoang, and M. Razeghi, Appl. Phys. Lett. **105**(12), 121104 (2014); A. Soibel, D. Z. Ting, C. J. Hill, A. M. Fisher, L. Hoglund, S. A. Keo, and S. D. Gunapala, *ibid.* **109**(10), 103505 (2016).

[2]D. Z. Ting, A. Soibel, and S. D. Gunapala, Infrared Phys. Technol. **84**, 102 (2017); I. Vurgaftman, G. Belenky, Y. Lin, D. Donetsky, L. Shterengas, G. Kipshidze, W. L. Sarney, and S. P. Svensson, Appl. Phys. Lett. **108**(22), 222101 (2016).

[3]G. Belenky, D. Donetsky, G. Kipshidze, D. Wang, L. Shterengas, W. L. Sarney, and S. P. Svensson, Appl. Phys. Lett. **99**(14), 141116 (2011).

[4]G. Belenky, Y. Lin, L. Shterengas, D. Donetsky, G. Kipshidze, and S. Suchalkin, Electron. Lett. **51**(19), 1521 (2015); S. P. Svensson, W. L.

Sarney, D. Donetsky, G. Kipshidze, Y. X. Lin, L. Shterengas, Y. Xu, and G. Belenky, Appl. Opt. **56**(3), B58 (2017).

[5]G. W. Winkler, Q. S. Wu, M. Troyer, P. Krogstrup, and A. A. Soluyanov, Phys. Rev. Lett. **117**(7), 076403 (2016).

[6]S. Suchalkin, G. Belenky, M. Ermolaev, S. Moon, Y. X. Jiang, D. Graf, D. Smimov, B. Laikhtman, L. Shterengas, G. Kipshidze, S. P. Svensson, and W. L. Sarney, Nano Lett. **18**(1), 412 (2018).

[7]S. Suchalkin, J. Ludwig, G. Belenky, B. Laikhtman, G. Kipshidze, Y. Lin, L. Shterengas, D. Smirnov, S. Luryi, W. L. Sarney, and S. P. Svensson, J. Phys. D: Appl. Phys. **49**(10), 105101 (2016).

[8]B. Laikhtman, S. Suchalkin, and G. Belenky, Phys. Rev. B **95**(23), 235401 (2017).

[9]F. Fuchs, E. Ahlswede, U. Weimar, W. Pletschen, J. Schmitz, M. Hartung, B. Jager, and F. Szmulowicz, Appl. Phys. Lett. **73**(25), 3760 (1998).

[10]P. Voisin, G. Bastard, and M. Voos, Phys. Rev. B **29**(2), 935 (1984).

[11]B. Jogai and D. N. Talwar, Phys. Rev. B **54**(20), 14524 (1996); I. Vurgaftman, J. R. Meyer, and L. R. Ram-Mohan, J. Appl. Phys. **89**(11), 5815 (2001).

[12]T. Andlauer and P. Vogl, Phys. Rev. B **80**(3), 035304 (2009).

[13]B. H. Hong, S. I. Rybchenko, I. E. Itskevich, S. K. Haywood, R. Intartaglia, V. Tasco, G. Raino, and M. De Giorgi, Phys. Rev. B **79**(16), 165323 (2009).

[14]W. L. Sarney, S. P. Svensson, M. K. Yakes, Y. Xu, D. Donetsky, and G. Belenky, J. Appl. Phys. **124**, 035304 (2018).

[15]Y. Jiang, S. Thapa, G. D. Sanders, C. J. Stanton, Q. Zhang, J. Kono, W. K. Lou, K. Chang, S. D. Hawkins, J. F. Klem, W. Pan, D. Smirnov, and Z. Jiang, Phys. Rev. B **95**(4), 045116 (2017).

[16]A. Leuliet, A. Vasanelli, A. Wade, G. Fedorov, D. Smirnov, G. Bastard, and C. Sirtori, Phys. Rev. B **73**(8), 085311 (2006).